Synthesis of Zeolite Bayah Nanocomposites with Metal Oxides Using Hydrothermal Method as Aquathermolysis Catalysts for Enhanced Oil Recovery Technology

Nailatul Eka Fadhillah, Muhammad Hasbi Ar-Raihan, Tirta Rona Mayangsari*

Department of Chemistry, Universitas Pertamina, Jakarta 12220, Indonesia
*Corresponding Author: tirta.rm@universitaspertamina.ac.id
Received: 29 Agustus 2024
Accepted: 21 Mei 2025

Abstracts

Heavy oil, a significant portion of global oil reserves, presents challenges in recovery due to its high viscosity and complex composition. Enhanced Oil Recovery (EOR) methods, such as aquathermolysis, have been developed to improve oil mobility by breaking down heavy hydrocarbons. Catalysts can significantly enhance aquathermolysis efficiency by accelerating reactions and minimizing repolymerization. In this study, ZnO and Fe_2O_3 nanoparticles, as well as their respective nanocomposites with activated zeolite, were synthesized via the hydrothermal method and evaluated as aquathermolysis catalysts. Characterization using FTIR, SEM, and XRD confirmed successful synthesis and nanoscale properties of the materials, with ZnO forming nanorods (80–100 nm) and Fe_2O_3 forming small granules (56.5–59.5 nm). Aquathermolysis tests conducted at 200°C demonstrated significant reductions in heavy oil viscosity at 40°C: 69.27% for ZnO/Activated zeolite and 71.57% for Fe_2O_3/Activated zeolite. The superior performance of Fe_2O_3/Activated zeolite is attributed to its macroporous structure and enhanced catalytic activity. These findings highlight the potential of these nanocomposites as efficient catalysts for EOR applications.

Keywords: Aquathermolysis, EOR, hydrothermal, iron oxide, zinc oxide

Introduction

Currently, Indonesia's energy sources still heavily rely on conventional oil, the availability of which is steadily decreasing in reservoirs. To address this issue, the oil industry has shifted its focus to the exploitation of heavy (non-conventional) oil, which constitutes approximately 70% of reservoir availability [1]. However, the exploitation of non-conventional oil tends to be more challenging because non-conventional oil has a higher viscosity compared to conventional oil, making the process of pumping oil from the reservoir to the surface difficult and production costs very high. Therefore, there is a need for cost-effective technology that minimizes environmental impact while enhancing the production of non-conventional oil, specifically through the use of Enhanced Oil Recovery (EOR) technology [2].

EOR can be implemented through various methods, including thermal recovery, miscible gas injection, and chemical injection [3]. One of the most widely used EOR methods is thermal recovery, which involves injecting superheated substances such as hot steam or hot water into the reservoir. Additionally, thermal recovery can be conducted through in-situ combustion within the reservoir itself to reduce the viscosity of heavy oil and decrease the surface tension between the rock and the oil, thereby increasing the mobility of the oil toward the production well [4].

Aquathermolysis is a thermal process that reduces heavy oil viscosity by breaking down large hydrocarbon molecules, particularly those containing heteroatoms like sulfur, oxygen, and nitrogen. This is facilitated by reactive H_2O, often under conditions enhanced by specific catalysts such as zeolite. This process cleaves

bonds such as C–S, C–O, and C–N, leading to the formation of lighter hydrocarbons and gases, thereby enhancing oil mobility [5], [6]. However, aquathermolysis alone can be time-consuming and may result in repolymerization of decomposed components back into heavy fractions, diminishing its effectiveness. To address this, catalysts are introduced to accelerate the reaction, minimize repolymerization, and further reduce viscosity. Appropriate catalysts facilitate stages like pyrolysis, hydrogenation, and ring-opening, enhancing the overall efficiency of the aquathermolysis process [7].

Many studies have discussed catalysts that can enhance the aquathermolysis process, one of which involves the use of nanoparticle catalysts [8]. The advantage of nanoparticle catalysts is their relatively high surface area, which can increase the reactivity and interaction between the catalyst particles and the oil [9]. Additionally, nanoparticle catalysts can be regenerated after being used in the aquathermolysis reaction [10]. Nassar et al. conducted research using nanocatalyst materials NiO, Fe_3O_4, and CO_3O_4, which showed that each catalyst could reduce the viscosity of heavy oil by 37%, 32%, and 21%, respectively. Among these nanocatalysts, NiO exhibited better catalytic properties in the processes of gasification, oil cracking, and reducing asphaltene content [11]. However, NiO has the drawback of being quite hazardous to the environment and toxic to humans [12]. Chen et al. synthesized a water-soluble Fe(III) complex using hydroxyl carbonyl acid and simple iron salts, which demonstrated a reduction in heavy oil viscosity by 80.1% during the aquathermolysis process at 180°C for 24 hours [13]. Yun-Rui conducted research using oil-soluble iron oleate, which showed a reduction in heavy oil viscosity by 86.1% at a concentration of 10% at 200°C [14]. Yasser I. et al. studied the use of water-soluble $Ni(CH_3COO)_2$ and $Zn(CH_3COO)_2$ in the aquathermolysis of heavy oil samples, conducted in a batch reactor at 300°C for 24 hours, which reduced the viscosity of heavy oil by 58% and 48%, respectively [15]. Nanocomposites can also increase the efficiency of the aquathermolysis process. Ferry Iskandar reported research using α-Fe_2O_3/Zeolite nanocomposites, which showed a reduction in heavy oil viscosity of up to 65.96% [16]. Zeolite can be used as a catalyst because it has Bronsted acid sites that serve as proton (H^+) sources in the aquathermolysis reaction and its microporous structure provides ample space for the reaction to occur, allowing the reaction to proceed at higher pressures [17], [18].

Based on the various catalysts presented, this research focuses on the synthesis of Fe and Zn metal oxide nanocomposite catalysts using natural zeolite from Bayah District, Lebak Regency, Banten Province, due to its abundant availability, ease of synthesis, and cost-effectiveness. The nanocomposite synthesis was carried out using the hydrothermal method with $ZnCl_2$ as the precursor for ZnO metal oxide synthesis and $FeCl_3.6H_2O$ as the precursor for Fe_2O_3 synthesis. The advantages of the hydrothermal method include the ability to control stoichiometry at low temperatures, resulting in high-purity products, the production of stable nanomaterials at high temperatures, and environmental friendliness [17].

Material and Methods

Synthesis of Active Zeolite Nanoparticles

The synthesis of zeolite nanoparticles was carried out using a top-down method with a ballmill. Subsequently, the zeolite was further ground using an agate mortar and sieved with a 200 mesh. The zeolite samples were then heated in a furnace at 400°C for 60 minutes.

Synthesis of Nanoparticles and Nanocomposites

The nanoparticles and nanocomposites were synthesized using the hydrothermal method at 190°C for 5 hours. Initially, $ZnCl_2$ (2.729 g) or $FeCl_3{\cdot}6H_2O$ (4.3248 g) was dissolved in distilled water (50 mL for $ZnCl_2$, 40 mL for $FeCl_3{\cdot}6H_2O$) and stirred at 600 rpm. Subsequently, a 0.5 M NaOH solution was added dropwise at a rate of 20 drops/min until the pH reached 10, followed by continuous stirring for 1 hour to maintain the pH. The solution was then

transferred to a Teflon autoclave for the hydrothermal process. After cooling to room temperature, the resulting precipitates—ZnO (white) or Fe_2O_3 (red)—were washed with distilled water and ethanol, dried in an oven at 80°C, ground with an agate mortar, sieved (200 mesh), and heated in a furnace at 400°C (3 hours for ZnO, 4 hours for Fe_2O_3).

For the synthesis of nanocomposites, activated zeolite was prepared by heating at 400°C for 60 minutes. The activated zeolite was combined with $ZnCl_2$ (2.183 g) or $FeCl_3 \cdot 6H_2O$ (4.3248 g) in distilled water (40 mL), and the procedure was repeated as described for the nanoparticles. The resulting precipitates—ZnO/Activated zeolite (gray) or Fe_2O_3/Activated zeolite (reddish-brown)—underwent similar washing, drying, grinding, sieving, and heating steps.

Catalyst Material Characterization

The catalyst material was characterized using Fourier Transform Infrared Spectroscopy (Nicolet iS5) with the Attenuated Total Reflectance (ATR) method in the wavenumber range of 4000-650 cm^{-1} to identify the chemical functional groups on the catalyst. X-Ray Diffraction (Smartlab Rigaku) was then performed using an X-ray source (CuKα) with an X-ray wavelength of 1.54060 Å to identify the phases and crystal structure of the catalyst material. Subsequently, SEM-EDS characterization was conducted to identify the nanocomposite catalyst's morphology, particle size, and composition.

Aquathermolysis of Crude Oil

The aquathermolysis process of crude oil was carried out using the hydrothermal method at a temperature of 200°C for 6 hours, using crude oil samples from the Lirik Field, Riau Province. First, the crude oil samples were heated to a temperature of 45°C. After the crude oil samples melted, the aquathermolysis process continued with crude oil without a catalyst and crude oil with the addition of 0.3% catalysts ZnO, ZnO/Activated zeolite, Fe_2O_3, and Fe_2O_3/Activated zeolite, with a heavy oil to distilled water ratio of 6:1 in a teflon autoclave. Subsequently, the viscosity of the crude oil was tested at varying temperatures of 60°C, 50°C, and 40°C using a NDJ-8S Digital Rotary Viscometer.

Results and Discussion

Characterization of Materials

Figure 1, A shows the FTIR characterization results for zeolite samples before and after activation. In the natural zeolite, functional groups from Si-O-Al bonds are present at a wavenumber of 1013 cm^{-1} and Al-O at 837 cm^{-1}. Additionally, at wavenumbers 2927 cm^{-1} and 1400 cm^{-1}, CH_2 and CH functional groups are observed as contaminants originating from the environment, specifically organic waste [19]. In the region of 3400-3700 cm^{-1}, there are broad O-H vibrations from water molecules, indicating that the natural zeolite has a hydrophilic nature. In contrast, the FTIR characterization results of the activated zeolite show a significant reduction in water molecules in the 3400-3700 cm^{-1} region. This is influenced by the high activation temperature of the natural zeolite, indicating a decrease in its hydrophilic properties. Furthermore, the Si-O-Al vibration shifts from a wavenumber of 1013 cm^{-1} to 982 cm^{-1}, accompanied by a shift in the Al-O/Si-O wavenumber from 837 cm^{-1} to 785 cm^{-1}, due to the removal of carbon and H_2O contaminants as a result of the activation temperature. Then, Fig. 1B shows the FTIR characterization results of the ZnO/Activated zeolite, indicating the presence of Si-OH at a wavenumber of 1632 cm^{-1}, which corresponds to O-H stretching vibrations due to high-temperature heating. Additionally, Si-O-Si is observed at a wavenumber of 1038 cm^{-1} and Si-O-Al at a wavenumber of 849 cm^{-1}. Meanwhile, Fig. 1C shows the FTIR characterization results for the Fe_2O_3/Activated zeolite, where the Si-OH functional group is present at a wavenumber of 1640 cm^{-1} and Si-O-Al at a wavenumber of 1015 cm^{-1}. The shift in wavenumbers for the Si-OH and Si-O-Al functional groups is attributed to the relatively high water content in the Fe_2O_3/Activated zeolite, as observed at a wavenumber of 3408 cm^{-1}. This high water content can be explained

by the microporous structure of zeolites, which traps water molecules within the framework even after heating at 400°C. While loosely bound water is removed during activation, tightly bound water or structural water can persist, as higher temperatures (e.g., 600–800°C) are required for complete dehydration. Additionally, the hydrophilic nature of zeolites, due to polar Si-OH and Al-OH groups, allows for re-adsorption of atmospheric moisture during storage or handling.

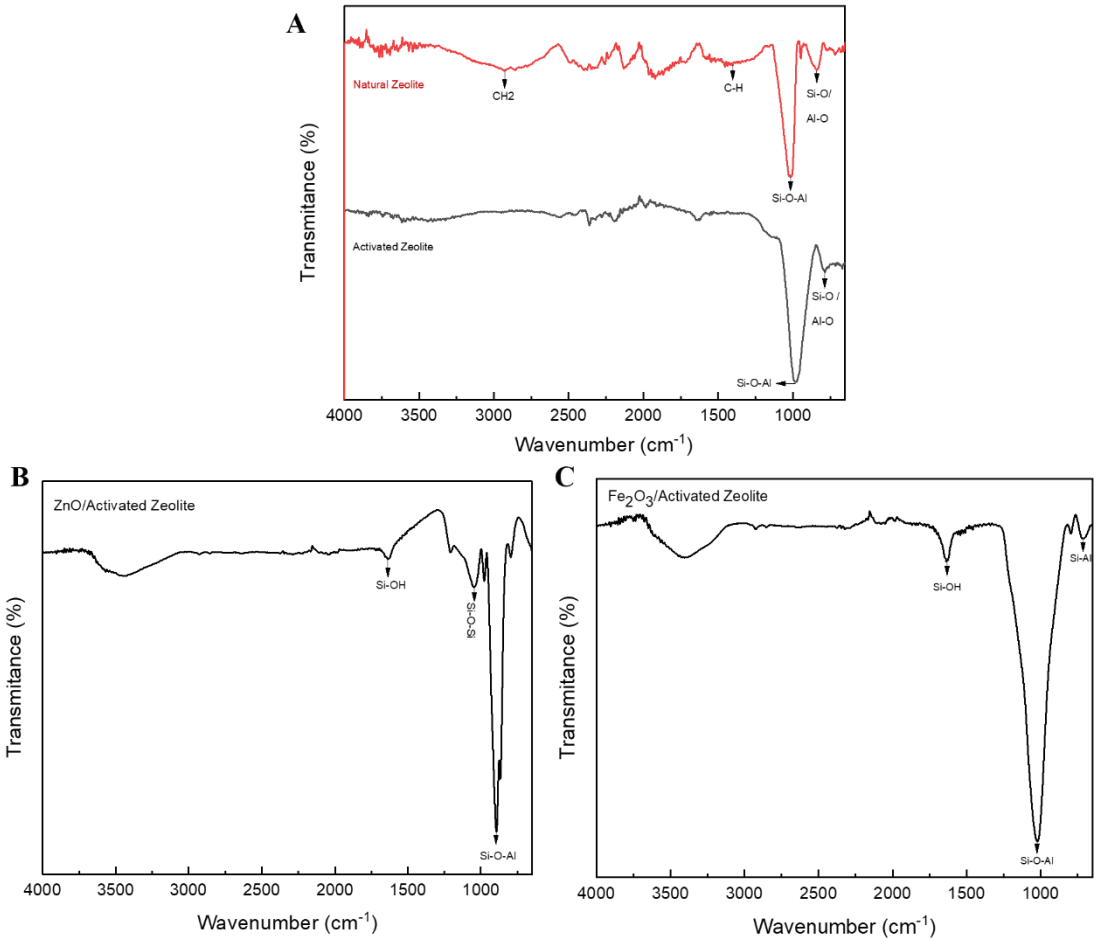

Figure 1. FTIR Characterization Results of; (A) Activated zeolit, (B) ZnO/Activated zeolit, and (C) Fe_2O_3/Activated zeolite

The XRD characterization results provide detailed information on the relationship between intensity and the 2θ angle, presented in the form of a diffractogram. Figure 2 shows the diffractograms for (A) activated zeolite, (B) ZnO, (C) ZnO/Activated zeolite, and (D) Fe_2O_3/Activated zeolite. The identified peaks, corresponding crystal phases, and planes are summarized in Table 1.

For activated zeolite (Figure 2A), three mixed mineral structures—clinoptilolite, sanidine, and mordenite—were identified. The prominent diffraction peaks at 11.17°, 13.41°, and 25.63° are characteristic of these phases. For ZnO (Figure 2B), distinctive peaks at 31.76°, 34.41°, and 36.23° confirm a hexagonal wurtzite structure as per JCPDS data. The ZnO/Activated zeolite composite (Figure 2C) exhibits diffraction peaks from both zeolite and ZnO, indicating

successful composite formation. Similarly, the Fe_2O_3/Activated zeolite composite (Figure 2D) demonstrates characteristic peaks for natural zeolite alongside Fe_2O_3 diffraction patterns. The results are detailed below:

Table 1. Summary of XRD Characterization Results

Material	2θ Peaks (°)	Identified Phases	Crystal Planes (hkl)	Notes
Activated zeolite (A)	11.17, 13.41, 15.26, 17.32, 20.95, 22.45	Clinoptilolite (C)	-	Mixed mineral structure of clinoptilolite, sanidine, and mordenite; high crystallinity (FWHM = 0.2251).
	19.60, 27.65, 36.96	Sanidine (S)	-	
	25.63, 26.26, 30.11, 32.68, 34.88, 35.72	Mordenite (M)	-	
ZnO (B)	31.76, 34.41, 36.23, 47.53, 56.57, 62.84, 67.93, 69.06	Pure ZnO	(100), (002), (101), (102), (110), (103), (112), (201)	Hexagonal wurtzite structure; identified from JCPDS data.
ZnO/Activated zeolite (C)	12.59, 21.94	Clinoptilolite (C)	-	Combination of natural zeolite and ZnO peaks.
	25.42	Mordenite (M)	-	
	31.41, 33.85, 38.71, 48.73, 65.37	ZnO	(100), (002), (101), (101), (200)	
Fe_2O_3/Activated zeolite (D)	11.08, 13.52, 15.36, 17.29, 19.68, 22.19, 25.76, 27.73, 30.11, 32.17, 35.94	Natural Zeolite	-	Fe_2O_3 peaks combined with natural zeolite phases.
	47.22, 48.52, 63.14	Fe_2O_3	-	

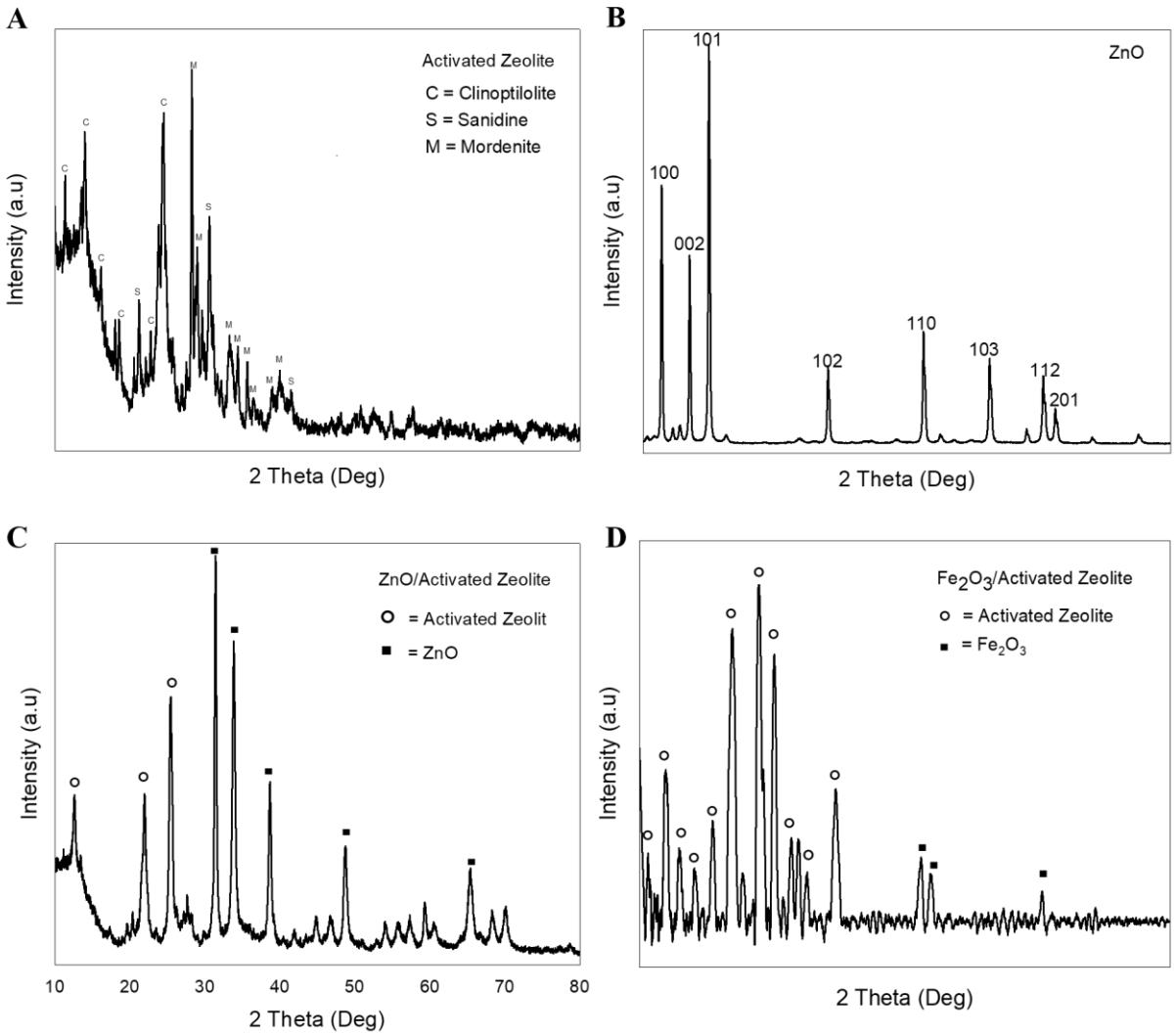

Figure 2. XRD Characterization Results of Catalyst Materials: (A) Activated zeolite; (B) ZnO nanoparticles, (C) ZnO/Activated zeolite composite, (D) Fe_2O_3/Activated zeolite

The determination of crystallite size of catalyst materials can be performed using the Scherrer equation (4.6)

$$D = \frac{K\lambda}{\beta \, Cos \, \theta} \qquad (4.6)$$

Where (K) is the Scherrer constant (0.9), λ is the wavelength of the X-ray used, β is the FWHM of the peak, and θ is the Bragg angle [20]. Based on the crystallite size calculations using the Scherrer equation, the average crystallite size of natural zeolite is 12.89 nm. The average crystallite size of ZnO is 37.95 nm, and the average crystallite size of the ZnO/Natural Zeolite composite is 15.01 nm. Additionally, the average crystallite size of the Fe_2O_3/Natural Zeolite composite is 13.88 nm. These calculations indicate that the crystallite sizes of the catalysts are in the nanocrystal range, as they fall within the 1-100 nm range [18].

In this study, SEM characterization were conducted on ZnO and Fe_2O_3 at magnifications of 7,500x and 10,000x. In Fig. 3, the morphology of ZnO particles appears as nanorods with diameters ranging from 80-100 nm, predominantly growing horizontally. In contrast, the morphology of Fe_2O_3 particles appears as small granules that agglomerate and grow in an orderly manner, with diameters ranging from 56.5-59.5 nm. This indicates that the particle

sizes of ZnO and Fe_2O_3 are in the nano range, as they fall within the 1-100 nm range, confirming the successful synthesis of nanoparticles [18].

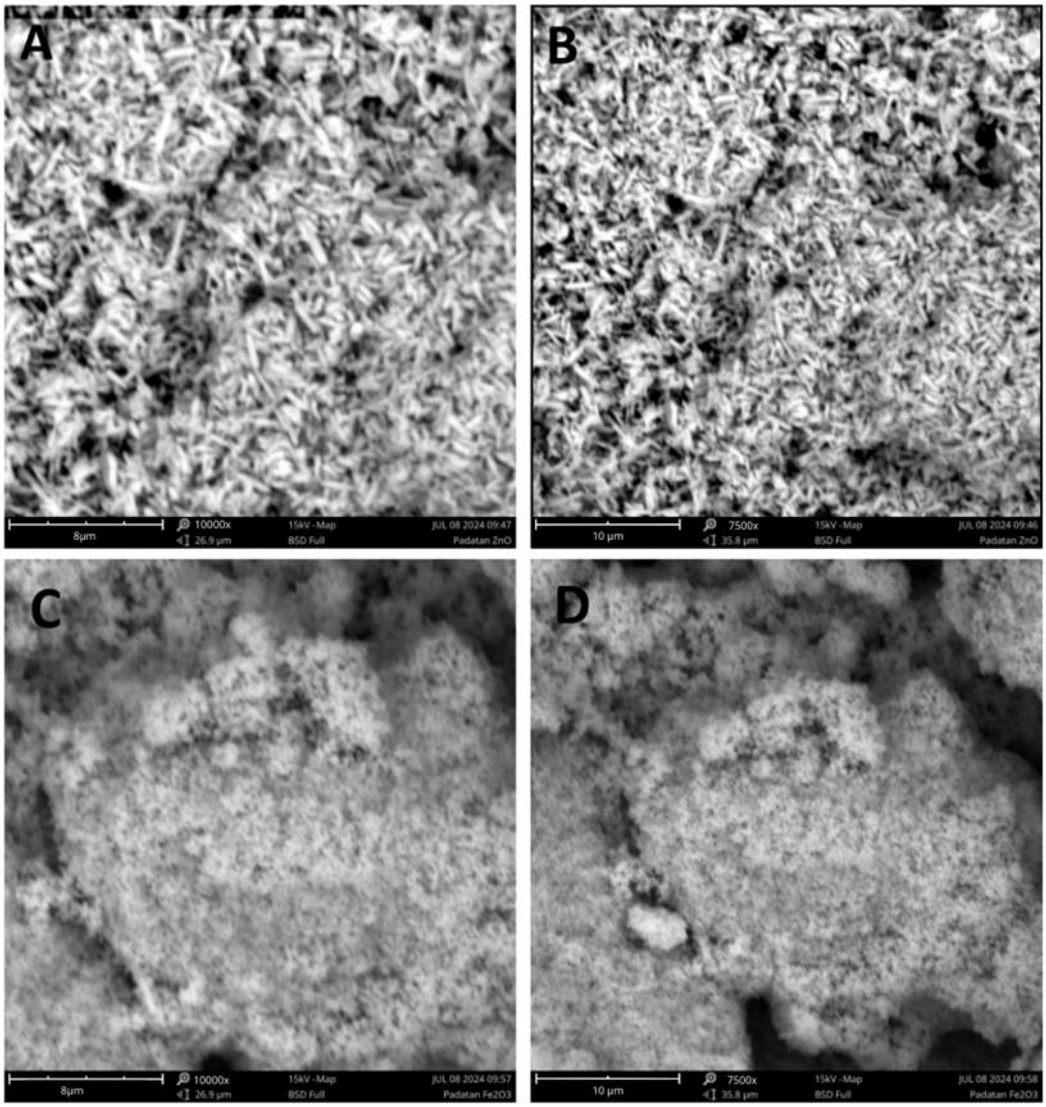

Figure 3. SEM Characterization Results of ZnO at 10,000 x Magnification (A), ZnO at 7,500x Magnification (B), Fe_2O_3 at 10,000x Magnification (C), and Fe_2O_3 at 7,500x Magnification (D)

The SEM-EDS analysis (Figures 4 and 5) highlights key differences between the ZnO/Activated zeolite and Fe_2O_3/Activated zeolite composites. In the ZnO composite (Figure 4), the zeolite appears as clumps with sizes ranging from 2.15 to 2.35 µm, while the ZnO particles are smaller, measuring between 0.89 and 0.95 µm. The EDS results confirm a high concentration of Zn (19.46%) and O (59.68%), alongside contributions from Si (14.71%) and Al (3.63%), indicating successful incorporation of ZnO into the zeolite. In contrast, the Fe_2O_3 composite (Figure 5) shows smaller zeolite clumps (0.29–0.34 µm) surrounded by irregular Fe_2O_3 particles, which are even smaller, ranging from 0.14 to 0.16 µm. Notably, macropores (0.18–0.27 µm) on the zeolite surface improve accessibility to the active sites. The EDS analysis supports this, with Fe (25.90%) and O (55.06%) dominating, while Si (13.64%) and Al (3.43%) are also present from the zeolite framework. However, the ZnO/Activated zeolite and Fe_2O_3/Activated zeolite composite particles are not nanosized, as their particle sizes exceed the

nanoparticle size range. This could be due to hydrothermal temperature and duration not being optimized for the natural zeolite, resulting in imperfect metal oxide distribution on the zeolite surface and causing agglomeration [21]. The Si and Al content in the synthesized composites indicates a high silica ratio, which, according to Bayu et al. (2018), provides advantages for catalytic applications by increasing resistance to high temperatures compared to low-silica zeolites [22]. This is attributed to the higher electronegativity of Si compared to Al, resulting in stronger Si-O-Si covalent bonds that require more energy to break. These findings, supported by Figures 4 and **5**, confirm the successful synthesis of both composites and their potential for aquathermolysis applications.

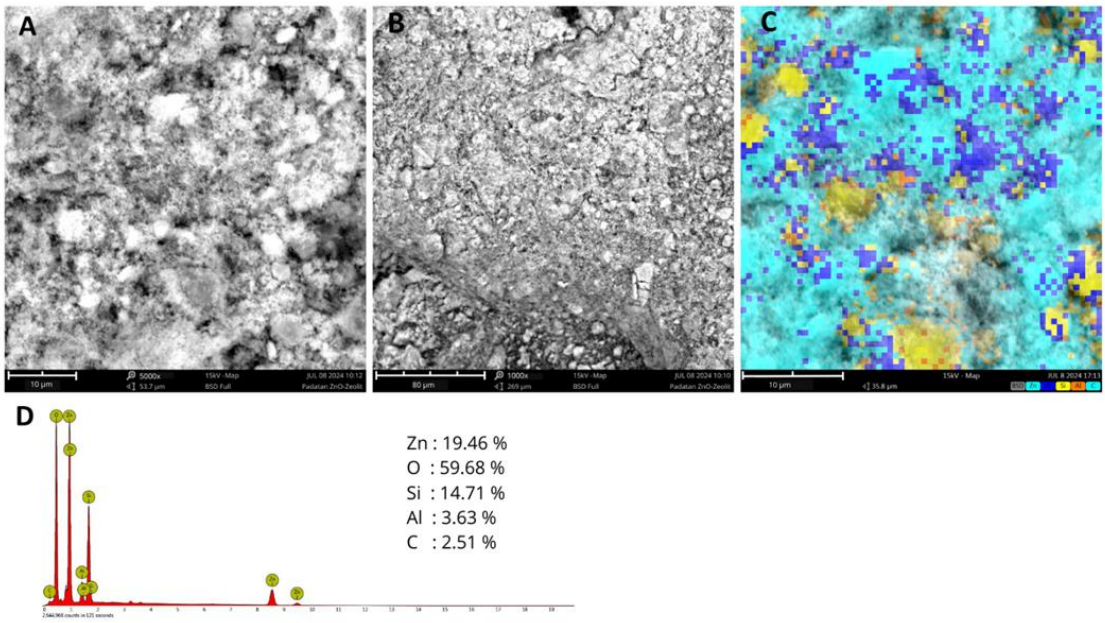

Figure 4. SEM-EDS Characterization Results of ZnO/Activated zeolite Composite at 5,000x Magnification (A), 1,000x Magnification (B), EDS Surface of ZnO/Activated zeolite (C), and Material Composition of ZnO/Activated zeolite Composite (D)

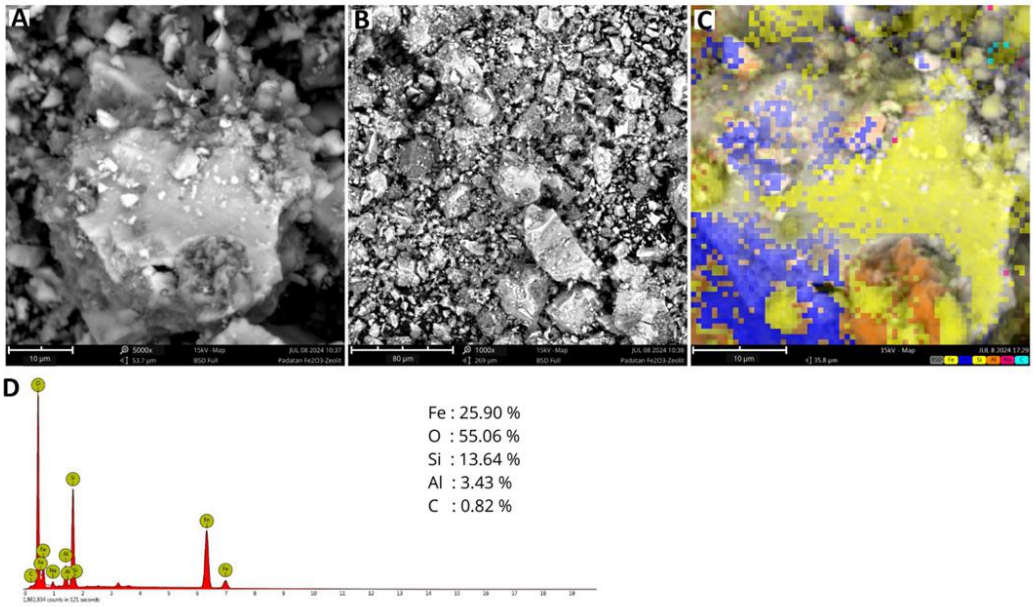

Figure 5. SEM-EDS Characterization Results of Fe_2O_3/Activated zeolite Composite at 5,000x Magnification (A), 1,000x Magnification (B), EDS Surface of Fe_2O_3/Activated zeolite (C), and Material Composition of Fe_2O_3/Activated zeolite Composite (D)

Aquathermolysis Testing

Aquathermolysis testing was conducted using FTIR with the Attenuated Total Reflectance (ATR) method, as shown in Fig. 6. We used an integrated peak area of corresponding absorbances to analyze the evolution of functional groups before and after the aquathermolysis process. At wavenumbers 2851-2919 cm^{-1}, there are C-H saturation bonds that influence the reduction of heavy oil viscosity, as saturated aliphatic hydrocarbons are more easily broken down into lighter fractions. Then, at wavenumbers 1376-1459 cm^{-1}, there are aromatic C-H bonds, whose presence is expected to have low absorption to enhance the energy value and quality of the oil. Additionally, at wavenumber 3445 cm^{-1} N-H bonds can cause polymerization in crude oil. At wavenumber 2200 cm^{-1} there is C≡N, at wavenumber 1746 cm^{-1} there is C=O, and at wavenumber 720 cm^{-1} there is paraffin, which affects the viscosity and density of crude oil [23].

The aquathermolysis reaction of crude oil was carried out using the hydrothermal method at 200°C for 6 hours. The catalyst was 0.3 wt%, and dynamic viscosity measurements were performed at varying temperatures of 60°C, 50°C, and 40°C. The success of aquathermolysis can be confirmed using FTIR by comparing the ratios of the crude oil group compositions, as shown in Table 2 The highest oil quality improvement was achieved from the aquathermolysis process using the Fe_2O_3/Natural Zeolite catalyst, with an increase in the C-H (Saturation)/Paraffin ratio of 16.0947 and the C-H (Saturation)/C-H (Aromatic) ratio of 30.2335. Additionally, ZnO/Natural Zeolite also contributed to reducing the viscosity of heavy oil, as evidenced by an increase in the C-H (Saturation)/Paraffin ratio of 16.075 and the C-H (Saturation)/C-H (Aromatic) ratio of 30.2719. The increase in the C-H saturation ratio in the oil indicates that the aquathermolysis process occurs in the pyrolysis and hydrogenation reaction sections, as shown in Fig. 7.

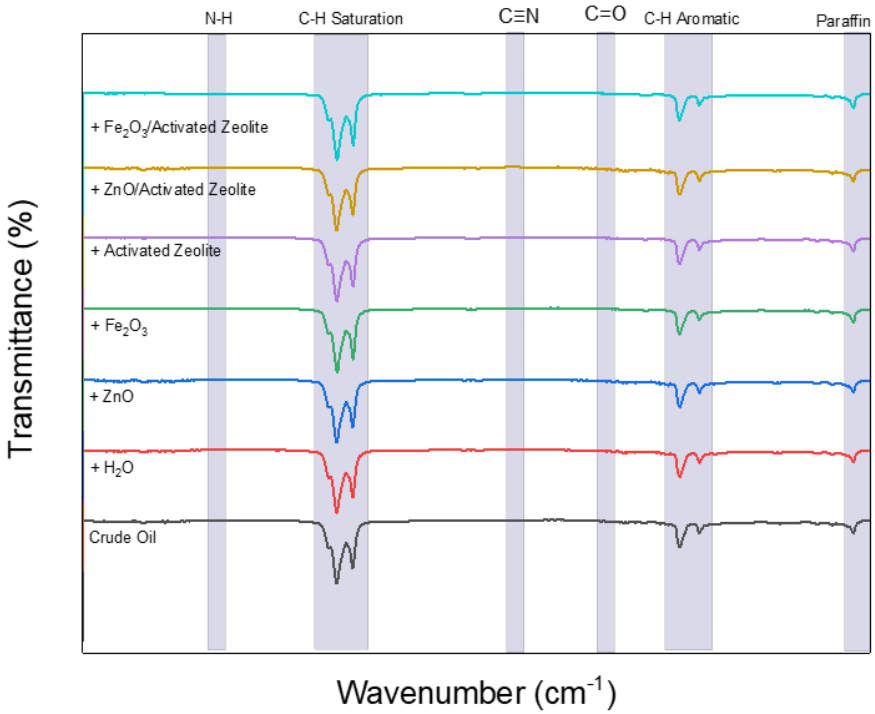

Figure 6. Aquathermolysis FTIR Crude Oil Results

Table 2. Comparison of Crude Oil Composition

Sample	C-H(Saturation)/Paraffin	C-H(Saturation)/C-H (Aromatic)
Crude Oil	1.5673	2.0510
Aquathermolysis without catalyst	1.5684	2.0513
Aquathermolysis + Activated Zeolite	16.0553	30.2219
Aquathermolysis + ZnO	1.5825	2.9692
Aquathermolysis + ZnO/Activated zeolite	16.075	30.2719
Aquathermolysis + Fe_2O_3	16.0947	30.2335
Aquathermolysis + Fe_2O_3/Activated zeolite	16.2562	30.4710

In Table 2 a significant reduction in oil viscosity is observed at 40°C, specifically during the aquathermolysis process with natural zeolite at 51.15%, aquathermolysis with ZnO/Activated zeolite at 69.27%, and aquathermolysis with Fe_2O_3/Activated zeolite at 71.57%. The highest percentage reduction in oil viscosity occurs during the aquathermolysis process with Fe_2O_3/Activated zeolite catalyst. This is because the Fe_2O_3/Activated zeolite material contains macropores on the zeolite surface, which increases oil accessibility and allows larger molecules in the oil to more easily reach the active sites of the catalyst. Additionally, the relatively small particle and crystal sizes of Fe_2O_3/Activated zeolite also contribute to the significant reduction in oil viscosity, as the larger surface area of the catalyst allows for more active sites to interact with the oil [21].

Table 3. Result of Crude Oil Viscosity Reduction

Sample	Viscosity (Pa.s)			Decline Percentage at Temperature 40 ^{0}C
	60 ^{0}C	50 ^{0}C	40 ^{0}C	
Crude Oil	0.0176	0.0271	0.0999	0 %
Aquathermolysis without catalyst	0.0155	0.0262	0.0500	49.95 %
Aquathermolysis + ActivatedNatural Zeolite	0.0145	0.025	0.0488	51.15%
Aquathermolysis + ZnO	0.0148	0.0257	0.0491	50.85 %
Aquathermolysis+ ZnO/ActivatedNatural Zeolite	0.0245	0.022	0.0307	69.27 %
Aquathermolysis + Fe_2O_3	0.013	0.0228	0.0458	54.15%
Aquathermolysis + Fe_2O_3/Activated zeolite	0.0129	0.022	0.0284	71.57%

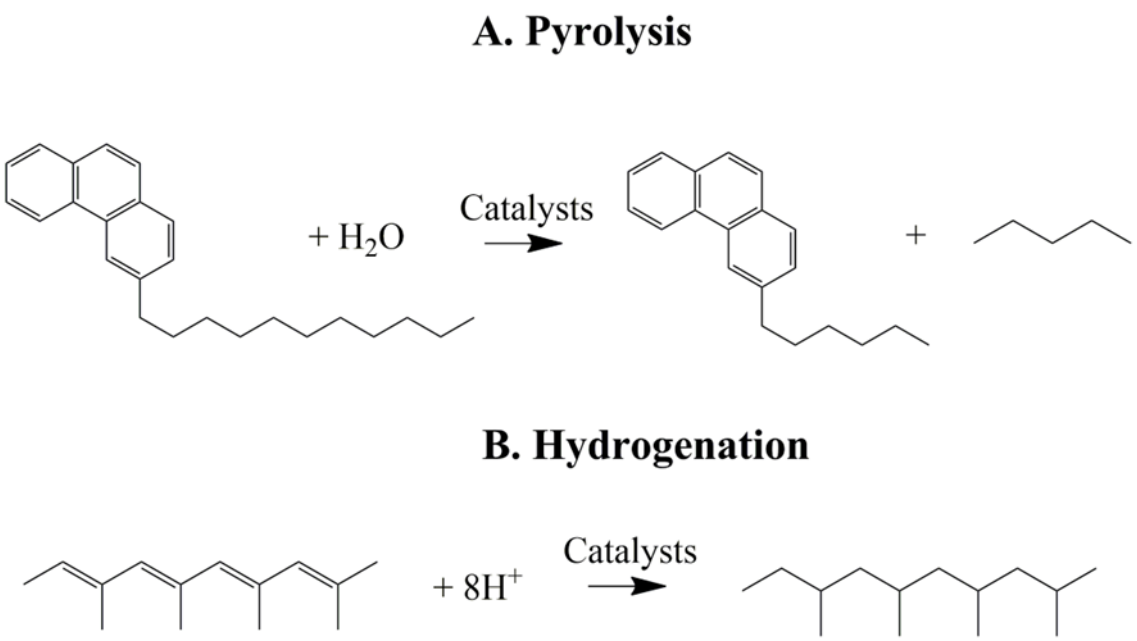

Figure 7. Pyrolysis Reaction (A) and Hydrogenation Reaction (B) in the Crude Oil Aquathermolysis Process [12]

The pyrolysis reaction likely occurs during the aquathermolysis process, where the bonds in heavy oil molecules begin to weaken due to high temperatures, shown in Figure 7. The presence of H_2O molecules helps break the C-C covalent bonds in heavy oil because H_2O can release H^+ ions that function to passivate the broken C-C bonds [19]. Meanwhile, the hydrogenation reaction of heavy oil occurs when the C=C bonds are broken into single C-C bonds due to the addition of hydrogen atoms from the catalyst and water to the C=C atoms [10]. The interaction between the catalyst and heavy oil indicates that the catalyst tends to be oil-soluble, thereby increasing the catalyst's effectiveness in reducing the viscosity of heavy oil [13].

Conclusion

This study successfully synthesized ZnO and Fe_2O_3 nanoparticles and their respective nanocomposites with activated zeolite using the hydrothermal method. ZnO formed nanorods (80–100 nm), while Fe_2O_3 appeared as small granules (56.5–59.5 nm). The ZnO/Activated zeolite and Fe_2O_3/Activated zeolite composites demonstrated effective reduction of heavy oil viscosity, achieving reductions of 69.27% and 71.57%, respectively, at 40°C. The Fe_2O_3/Activated zeolite composite exhibited the best performance due to its macroporous structure and small particle size, which enhance oil accessibility and catalytic activity. These findings highlight the potential of these catalysts for improving Enhanced Oil Recovery (EOR) efficiency, with further work planned to evaluate their field-scale performance and long-term stability.

References

[1] B. Hascakir, "Introduction to Thermal Enhanced Oil Recovery (EOR) special issue," *J Pet Sci Eng*, vol. 154, pp. 438–441, Jun. 2017, doi: 10.1016/J.PETROL.2017.05.026.

[2] H. Schobert, *Chemistry of Fossil Fuels and Biofuels*. Cambridge University Press, 2021.

[3] K. Guo, H. Li, and Z. Yu, "In-situ heavy and extra-heavy oil recovery: A review," *Fuel*, vol. 185, pp. 886–902, Dec. 2016, doi: 10.1016/J.FUEL.2016.08.047.

[4] R. E. Correa Pabón and C. R. de Souza Filho, "Crude oil spectral signatures and empirical models to derive API gravity," *Fuel*, vol. 237, pp. 1119–1131, Feb. 2019, doi: 10.1016/J.FUEL.2018.09.098.

[5] S. Chen, S. Zhang, J. Feng, X. Long, T. Hu, and G. Chen, "Water-Soluble Fe(III) Complex Catalyzed Coupling Aquathermolysis of Water-Heavy Oil-Methanol," *Catalysts 2024, Vol. 14, Page 353*, vol. 14, no. 6, p. 353, May 2024, doi: 10.3390/CATAL14060353.

[6] Q. Wang *et al.*, "Synergistic Catalysis of Water-Soluble Exogenous Catalysts and Reservoir Minerals during the Aquathermolysis of Heavy Oil," *Molecules 2024, Vol. 29, Page 3761*, vol. 29, no. 16, p. 3761, Aug. 2024, doi: 10.3390/MOLECULES29163761.

[7] S. A. Sitnov *et al.*, "Underground Upgrading of the Heavy Crude Oil in Content-Saturated Sandstone with Aquathermolysis in the Presence of an Iron Based Catalyst," *Catalysts 2021, Vol. 11, Page 1255*, vol. 11, no. 10, p. 1255, Oct. 2021, doi: 10.3390/CATAL11101255.

[8] S. Kokal and A. Abdulaziz, "Enhanced Oil Recovery: Challenges & Opportunities | Request PDF." Accessed: Dec. 04, 2024. [Online]. Available: https://www.researchgate.net/publication/306150203_Enhanced_Oil_Recovery_Challenges_Opportunities

[9] E. M. A. Mokheimer, M. Hamdy, Z. Abubakar, M. R. Shakeel, M. A. Habib, and M. Mahmoud, "A comprehensive review of thermal enhanced oil recovery: Techniques evaluation," *Journal of Energy Resources Technology, Transactions of the ASME*, vol. 141, no. 3, Mar. 2019, doi: 10.1115/1.4041096/377484.

[10] O. Muraza and A. Galadima, "Aquathermolysis of heavy oil: A review and perspective on catalyst development," *Fuel*, vol. 157, pp. 219–231, Oct. 2015, doi: 10.1016/J.FUEL.2015.04.065.

[11] Nassar, Nashaat N., Hassan, Azfar., Pereira-Almao, Pedro. *Application of Nanotechnology for Heavy Oil Upgrading: Catalytic Steam Gasification/Cracking of Asphaltenes.*Energy Fuels.2011.

[12] C. Mateus-Rubiano, A. C. Castillo, P. León, L. Rueda, D. Molina V, and A. Y. Leon, "Effect of hydrotreatment process on the physicochemical properties of a Colombian heavy crude oil post-catalytic aquathermolysis," *Energy*, vol. 298, Jul. 2024, doi: 10.1016/j.energy.2024.131349.

[13] S. K. Maity, J. Ancheyta, and G. Marroquín, "Catalytic Aquathermolysis Used for Viscosity Reduction of Heavy Crude Oils: A Review," *Energy and Fuels*, vol. 24, no. 5, pp. 2809–2816, May 2010, doi: 10.1021/EF100230K.

[14] N. Eviva, A. Shofiyani, and E. Sayekti, "Synthesis of NaP Zeolite Based on Bauxite Red Mud Using Hydrothermal Method on Mole Ratio of SiO2/Al2O3 Variations," *POSITRON*, vol. 13, no. 1, p. 77, May 2023, doi: 10.26418/POSITRON.V13I1.60099.

[15] J. Li, Q. Wu, and J. Wu, "Synthesis of Nanoparticles via Solvothermal and Hydrothermal Methods," *Handbook of Nanoparticles*, pp. 1–28, 2015, doi: 10.1007/978-3-319-13188-7_17-1.

[16] G. Yang and S. J. Park, "Conventional and Microwave Hydrothermal Synthesis and Application of Functional Materials: A Review," *Materials 2019, Vol. 12, Page 1177*, vol. 12, no. 7, p. 1177, Apr. 2019, doi: 10.3390/MA12071177.

[17] Y. X. Gan, A. H. Jayatissa, Z. Yu, X. Chen, and M. Li, "Hydrothermal Synthesis of Nanomaterials," 2020, *Hindawi Limited*. doi: 10.1155/2020/8917013.

[18] M. Ahmed, "Nanomaterial synthesis," *Polymer Science and Nanotechnology: Fundamentals and Applications*, pp. 361–399, Jan. 2020, doi: 10.1016/B978-0-12-816806-6.00016-9.

[19] W. Zhang, Q. Li, Y. Li, S. Dong, S. Peng, and G. Chen, "Viscosity Reduction and Mechanism of Aquathermolysis of Heavy Oil Co-Catalyzed by Bentonite and Transition Metal Complexes," *Catalysts 2022, Vol. 12, Page 1383*, vol. 12, no. 11, p. 1383, Nov. 2022, doi: 10.3390/CATAL12111383.

[20] A. Monshi, M. R. Foroughi, M. R. Monshi, A. Monshi, M. R. Foroughi, and M. R. Monshi, "Modified Scherrer Equation to Estimate More Accurately Nano-Crystallite Size Using XRD," *World Journal of Nano Science and Engineering*, vol. 2, no. 3, pp. 154–160, Sep. 2012, doi: 10.4236/WJNSE.2012.23020.

[21] A. M. Famia and M. Muldarisnur, "Pengaruh Temperatur Sintesis Hidrotermal Terhadap Diameter Nanopartikel Seng Oksida," *Jurnal Fisika Unand*, vol. 8, no. 2, 2019.

[22] A. Bayu *et al.*, "SCIENCE & TECHNOLOGY Evaluation of Ball-Milling Process for the Production of Carbon Particles from Rice Straw Waste," *Pertanika J. Sci. & Technol*, vol. 26, no. 3, pp. 1373–1382, 2018, [Online]. Available: http://www.pertanika.upm.edu.my/

[23] V. Simanzhenkov and R. Idem, "Crude Oil Chemistry," *Crude Oil Chemistry*, Aug. 2003, doi: 10.1201/9780203014042.